Biochemistry and Biophysics Reports 29 (2022) 101198

Contents lists available at ScienceDirect

Biochemistry and Biophysics Reports

journal homepage: www.elsevier.com/locate/bbrep

Calmodulin binding to the dehydrogenase domain of NADPH oxidase 5 alters its oligomeric state

Dustin Smith [a], Laura Lloyd [a], Elaine Wei [c], Paria Radmanesh [a], Chin-Chuan Wei [a,b,*]

[a] Department of Chemistry, College of Arts and Sciences, Southern Illinois University Edwardsville, Edwardsville, IL, 62026, USA
[b] Department of Pharmaceutical Sciences, College of Pharmacy, Southern Illinois University Edwardsville, Edwardsville, IL, 62026, USA
[c] Department of Biochemistry, School of Molecular and Cellular Biology, University of Illinois, Urbana Champaign, IL, 61801, USA

ARTICLE INFO

Keywords:
Calcium binding
NADPH Oxidase 5
Calorimetry
Spectroscopy
Gel filtration

ABSTRACT

Superoxide generated by NADPH Oxidase 5 (Nox5) is regulated by Ca^{2+} through the interaction of its self-contained Ca^{2+} binding domain and dehydrogenase domain (DH). Recently, calmodulin (CaM) has been reported to enhance the Ca^{2+} sensitivity of Nox5 by binding to the CaM-binding domain sequence (CMBD), in which the interaction between CaM and Nox5 is largely unclear. Here, we used the CMBD peptide and truncated DH constructs, and separately studied their interaction with CaM by fluorescence, calorimetry, and dynamic light scattering. Our results revealed that each half-domain of CaM binds one CMBD peptide with a binding constant near 10^6 M^{-1} and a binding enthalpy change of −3.81 kcal/mol, consistent with an extended 1:2 CaM:CMBD structure. However, the recombinant truncated DH proteins exist as oligomers, possibly trimer and tetramer. The oligomeric states are concentration and salt dependent. CaM binding appears to stabilize the DH dimer complexed with CaM. The thermodynamics of CaM binding to the DH is comparable to the peptide-based study except that the near unity binding stoichiometry and a large conformational change were observed. Our result suggests that the oligomeric states of Nox5, mediated by its DH domain and CaM, may be important for its superoxide-generating activity.

1. Introduction

The NADPH Oxidase (Nox) enzymes are responsible for the production of reactive oxygen species (ROS) for cellular signaling, gene regulation, and host immunological defense [1]. However, an imbalance of cellular ROS production has been shown to be correlated with a variety of health complications such as cancer, as well as neurological, renal, and cardiovascular disorders [2–7]. Superoxide is one type of ROS produced primarily by Nox proteins. Several homologous enzymes have been identified, including Nox1-5 and Dual Oxidase (Duox) [8]. These Nox proteins are found in several tissues and have different activation mechanisms. Among them, Nox2 (phagocytic Nox) is well documented for its non-specific immunity by generating superoxide that kills invading pathogens. However, more recent evidence indicates that all non-phagocytic Nox enzymes play a role in cell defense in addition to their roles in mediating redox signaling to maintain healthy cells.

All Nox proteins share similar sequence features, consisting of a polypeptide homologous to $gp91^{phox}$ that contains a five-to-six transmembrane heme domain and a flavoprotein or dehydrogenase (DH) containing FAD and NADPH binding sites. An active complex formation from accessory and/or regulatory proteins are required for Nox1-3 while Nox4 is constitutively expressed as an activated form. Interestingly, superoxide and hydrogen peroxide production by Nox5 and Duox are Ca^{2+} dependent, through their additional self-contained N-terminal EF-hand domain (EFD) [9]. Nox5 overexpression results in high ROS production and has been reported to be associated with disease development, including hairy cell leukemia [2], prostate cancer [3], diabetic nephropathy [10], vascular diseases [5–7].

Though the Nox5's superoxide-generating mechanism is not completely understood, it is generally believed that Nox5's EFD, comprised of four EF-hand motifs (EFs), undergoes a Ca^{2+}-dependent conformational change to mediate the EFD-DH interaction. Such a domain-domain interaction is essential to allow electron transfer from NADPH to FAD, through the transmembrane hemes, and lastly ending up on molecular oxygen. Previously, we demonstrated that the C-terminal end of Ca^{2+}-bound EFD (Ca^{2+}-EFD) binds specifically to the regulatory EF-hand binding domain (REFBD) located in Nox5's DH using the REFBD peptide and truncated DH proteins [11]. The Ca^{2+}-mediated

* Corresponding author. Department of Chemistry, Southern Illinois University, Edwardsville, USA.
E-mail address: cwei@siue.edu (C.-C. Wei).

https://doi.org/10.1016/j.bbrep.2021.101198
Received 16 November 2021; Received in revised form 29 December 2021; Accepted 29 December 2021

domain-domain interaction is viewed as the main activation mechanism for Nox5. However, other proteins including calmodulin (CaM), tyrosine kinase, Hsp90, and caveolin have been reported to modulate the Nox5's superoxide-generating activity [12–15]. Among them, CaM is reported to enhance Nox5's Ca^{2+} sensitivity. The mechanism regarding the role of CaM in assisting Nox5 activity is attractive because it is believed that the Ca^{2+} level (0.1–1 μM) in the stimulated cells is not sufficient to activate Nox5 due to its weak Ca^{2+} binding affinity [12]. However, we determined that the Ca^{2+} binding constants (K_a) of EFD are in the range of 10^5–10^6 M^{-1} in physiological conditions, which is one order higher than the previous reported values [12]. In comparison, the Ca^{2+} binding for CaM is 10^4–10^5 M^{-1} [16]. Therefore, it is interesting that the Nox5 activity is regulated by two Ca^{2+}-dependent protein components when both share similarities in protein folds [11,17]. To enhance the Nox5's Ca^{2+} sensitivity, a synergy in increasing Ca^{2+} binding affinities for CaM and Nox5′EFD is expected for the activation at a lower Ca^{2+} concentration. In other words, the binding affinity of Ca^{2+} to Nox5's EFD (or CaM) increases in the presence of CaM (or Nox5's EFD). This hypothesis remains to be proven.

CaM and Nox5's EFD consist of four EF-hand motifs (EFs) that bind to four Ca^{2+} ions with their N-terminal lobe containing the 1st EF (EF1) and EF2 and the C-terminal half-domain containing EF3 and EF4. The half-domains are joined by a flexible linker region. CaM binds to a conserved sequence called the CaM-binding domain (CMBD) in the target enzymes. In Nox5, the CMBD sequence has been identified in the DH region [18]. In this study, we aimed to explore the potential binding mechanism of CaM to the DH of human Nox5β (hNox5) via isothermal titration calorimetry, dynamic light scattering, and fluorescence. To interrogate the role of CaM, we reported the binding thermodynamics of CaM with the CMBD peptide and truncated DH proteins. The results from this study are important to understand the role of CaM in Nox5 activity in future study.

2. Experimental

2.1. General

All chemicals were purchased from MilliporeSigma (St. Louis, MO) and ThermoFisher Scientific (Waltham, MA) without further purification. The human Nox5β′s CMBD peptide and the N-terminal Dansyl-labeled fluorescent peptide with the sequence $_{H2N}$RPDWSKVFQ KVAAEKKGKV$_{COOH}$ corresponding to 671–689 residues in a purity of >95% were purchased from Abclonal (Cambridge, MA). The purity of the proteins was estimated by SDS-PAGE electrophoresis and densitometry using UN-SCAN-IT software (Silk Scientific, *Inc.*, Utah). All proteins used in characterization have a purity >90%. All measurements were performed at least three times using two to three different protein batches, and the results are reproducible. When possible, the data presented here are the mean values plus the standard deviation.

2.2. Concentration determination

The concentrations of the peptide and protein containing a single Trp or Dansyl group were determined by using extinction coefficients (ε) of 5380 $M^{-1}cm^{-1}$ at 280 nm and 3400 $M^{-1}cm^{-1}$ at 338 nm for Trp and Dansyl group, respectively. An ε_{276} value of 2900 $M^{-1}cm^{-1}$ was used to calculate the CaM concentration [19]. The concentrations of the truncated DH proteins were determined by a Bradford assay (ThermoFisher). Concentrations were cross analyzed for validity when appropriate. For example, the determined concentration of CaM by extinction coefficient at 276 nm was checked against the determined concentration of Dansy-labeled CaM using extinction coefficient for Dansyl group.

2.3. Recombinant protein expression and purification

The recombinant 6xHis-tagged CaM, maltose binding protein (MBP), and MBP-fused DH proteins including the residues 665–719 ($DH_{665\text{-}719}$), $DH_{605\text{-}719}$, $DH_{584\text{-}719}$, and $DH_{528\text{-}719}$ were expressed and purified as described elsewhere [11] with some modification. Briefly, the *E. coli* cells containing the pMal-c2X plasmid with the DH gene inserted were grown and expressed in Luria Broth containing 2 g/L of glucose and 1 mM ampicillin; they were induced with 0.3–0.5 mM Isopropyl β-D-1-thiogalactopyranoside (IPTG) at OD_{600} = 0.4–0.6. The cells were pelleted after 18 h of growth at room temperature. The pellets were then sonicated and centrifuged at 15,000×*g* for 20 min. The resulting supernatant was loaded into a column containing 5 mL of diethylaminoethyl (DEAE) cellulose (MilliporeSigma) equilibrated with 50 mM Tris, 100 μM EDTA, pH 7.5 (Buffer A). After washing with 10 bed volumes of Buffer A, the desired DH protein was eluted with 2 bed volumes of Buffer A plus 0.5 M NaCl. The eluted fraction was mixed with an equal volume of Buffer A followed by loading it to an amylose column (New England BioLabs, Ipswich, MA). After washing with 3 bed volumes of Buffer CB (50 mM Tris, 0.2 M NaCl, 1 mM EDTA, pH 7.5.), a solution of Buffer CB containing 10 mM maltose was used to elute the MBP-fused DH. Lastly, the DH proteins were further purified with a CaM-immobilized column [11]. Note that MBP-fused DHs were used for characterization without the cleavage of MBP from DH due to the low solubility of the DH domain proteins.

The recombinant 6xHis-tagged CaM was first purified with a Pro-Bond Ni-NTA Resin column (ThermoFisher) followed by a Phenyl Sepharose column. The blue or cyan fluorescent protein (BFP or CFP) fused CaM (CaM-BFP or CaM-CFP) and its N- and C-terminal half domains of CaM (residues 1–75, NCaM and residues 76–149, CCaM) were prepared by cloning the corresponding CaM gene sequences into a pRSET-BFP or pRSET-CFP vector (ThermoFisher) immediately before the fluorescence proteins. The resulting plasmid was transformed to T7 or BL21(DE3) *E. Coli* cells (New England Biolabs) and the purification was identical to CaM. All purified proteins were stored at - 80°C until use or directly used after purification.

2.4. Pulldown experiments

To identify the protein constructs that bind CaM or its individual half-domains, three specific protein-immobilized columns were prepared using NHS-Activated Agarose Resin (ThermoFisher). To help visualize the immobilization, BFP- or CFP-fused CaM proteins were used intentionally. Briefly, 5 mg CaM-BFP, NCaM-CFP, or CCaM-BFP was buffer-exchanged three times with Coupling Buffer (0.1 M sodium phosphate, 0.15 M NaCl, pH 7.2) followed by a reaction with 2-mL of activated agarose in three separate columns (1 cm × 2 cm) for 1 h at room temperature. After washing with 4 mL of Coupling Buffer, the remaining unreactive sites in resin were quenched with 2 mL 1 M Tris, pH 7.5 followed by washing with 6 mL of Coupling Buffer. The columns were stored in 50 mM Tris, 100 μM EDTA, pH 7.5 at 4 °C.

The pulldown experiments were conducted by loading the DH proteins to the three columns equilibrated with Buffer B (50 mM Tris, 2 mM Ca^{2+}, pH 7.5). After washing the column with 10 mL of Buffer B, any retained protein then was eluted with 5 mL buffer containing 50 mM Tris, 5 mM EDTA, pH 7. All washing and eluted fractions from individual columns were concentrated and adjusted to a final volume of 1-mL for fair comparison on a 12–15% SDS-PAGE.

2.5. Spectroscopic measurements

Absorbance measurements were carried out using a UV-1800 Spectrometer (Shimadzu, Kyoto, Japan). The fluorescence spectra were recorded on the FluoroMax-3P or FluoroMax-4 (Horiba John Yvon, *Inc.*), equipped with a temperature control unit and polarizers. To monitor Tyr or Trp fluorescence, 2–5 μM of protein was excited at a wavelength of 280 or 295 nm. The excitation wavelength of 335 nm was used to monitor fluorescence from the Dansyl group. The slit widths of 2 and 5 nm for excitation and emission were chosen for intensity measurements

while the slit widths of 10 and 10 nm were used for the anisotropy measurement. For the binding study of CaM and CMBD using Trp fluorescence, the emission spectra of CMBD alone and with different concentrations of CaM were recorded. These spectra were then corrected from the spectra from a separated titration, in which the same amounts of CaM were titrated to the buffer at an identical setting, which are attributed from CaM's Tyrosine residues and water Raman. Unless indicated elsewhere, the buffer was 50 mM Tris, pH7.5 with 2 mM Ca^{2+} or 1 mM EDTA. The equations and fittings from intensity changes and anisotropy values were conducted as described previously [11].

2.6. Isothermal titration calorimetry (ITC)

All ITC experiments were run on a VP-ITC (GE, Pittsburgh, PA) as described elsewhere [20]. Typically, the ITC measurement was set for 5 or 10 μL injections dispensed over 10 or 20 s, respectively, with 120 s spacing. The concentrations of the protein/peptide in the sample cell ranged from 2 μM to 30 μM while the concentrations of the samples in the syringe ranged from 100 μM to 500 μM. The resulting ITC data was corrected for the heat of dilution from a control experiment, in which titrant was injected to sample cell containing buffer only. The buffer used was 50 mM Tris, 2 mM Ca^{2+}, pH 7.5 When studying salt-dependent binding, 0.15–0.25 M NaCl was included in the buffer. All data sets were fitted with the "One Set of Sites" fitting function.

2.7. Size-exclusion chromatography (SEC) or gel filtration chromatography

The oligomeric states of the proteins were monitored by a high-performance liquid chromatography system (HPLC; Shimazu, Inc., Kyoto, Japan) with a Shodex PROTEIN KW802.5 column (Showa Denko America, *Inc*, New York) controlled by LabSolutions software. The column was equilibrated with a buffer containing 20 mM Tris, 0.2–0.5 M NaCl, pH 7.5 with 2 mM Ca^{2+} or 1 mM EDTA. The settings for flow rate and the wavelength for UV detector were 1.0 mL/min and 280 nm, respectively. The protein samples were filtered through a 0.45 μm filter before injecting into a 20-μL sample loop. When the fraction collector was used, a calibrated delay of 330 μL was used for collecting fractions.

2.8. Dynamic light scattering (DLS)

The DLS experiments were performed on a DynaPro NanoStar (Wyatt Technology, Santa Barbara, CA). Prior to measurement, all samples were first filtered with a 0.45 μm filter followed by a 0.1 μm filter. Then, 20 μL of the filtered sample at the concentration of 1 mg/mL in 50 mM Tris, pH 7.5 was applied to a Wyatt disposable cuvette and left to equilibrate at 25 °C for 2 min. The acquisition time was set to 5 s and the minimum peak intensity was 1%. The intensity autocorrelation for low and high cut off times were 0.5 and 100,000 μs. The resulting autocorrelation functions were averaged 10 times to remove noise, which was fitted to the decaying exponential functions to determine the diffusion coefficient. The hydrodynamic radius (R_h) was calculated assuming the shape of molecules are spherical in all cases.

3. Results

3.1. Characterization of CaM with Nox5's CMBD peptide

3.1.1. Binding determined by fluorescence

The Nox5's CMBD contains a single Trp residue while it is absent in CaM, making the system suitable for binding study using Trp fluorescence. Previously, the binding for CaM and the CMBD peptide was estimated with a K_a value of 4 x 10^7 M^{-1} and near unity stoichiometry [18]. Those values were estimated by the titration curve with the inflection point to determine the binding stoichiometry-a practice that cannot determine the binding affinity precisely. Here we revisited the system with the spectral correction and fitted the titration with non-linear regression. Fig. 1A shows the corrected emission spectra of the CMBD peptide and its complex with difference amounts of CaM in the presence of Ca^{2+}. The CMBD peptide exhibits a maxima emission wavelength (λ_{em}) at 350 nm. Upon the addition of CaM, the fluorescence has a blue shift to 330 nm. The large wavelength shift (~20 nm) indicates the Trp residue of CMBD is changed to a buried non-polar environment, consistent with the K_{SV} values of 6.225 M^{-1} for CMBD and 0.726 M^{-1} for CaM/CMBD complex obtained from dynamic quenching with potassium iodide (See supplementary figure; Fig. S1). Our titration spectra roughly indicate that there are two distinct fluorescent species: the unbound CMBD peptide with λ_{max} = 352 nm and CaM-bound CMBD peptide with λ_{max} = 330 nm. We observed the isosbestic point at 352 nm, not 364 nm in the previous report [18]. By following the formation of the CaM/CMBD complex (i.e., monitoring at 330 nm), the titration requires nearly one equivalent of CaM to saturate the binding, and the fitting results in a K_a value of 1.71 × 10^7 M^{-1} in a 2:1 (CMBD:CaM) binding (Insert in Fig. 1A).

Because the CMBD peptide is much smaller than CaM, we monitored the complex formation by molecular tumbling using fluorescence anisotropy. The emission wavelength at 352 nm was chosen since there is no significant correction for quantum yields required for fitting and there is low signal attributed from CaM. The Trp anisotropy value (*r*) of the peptide alone was 0.0405. When a solution of 1 μM CMBD was

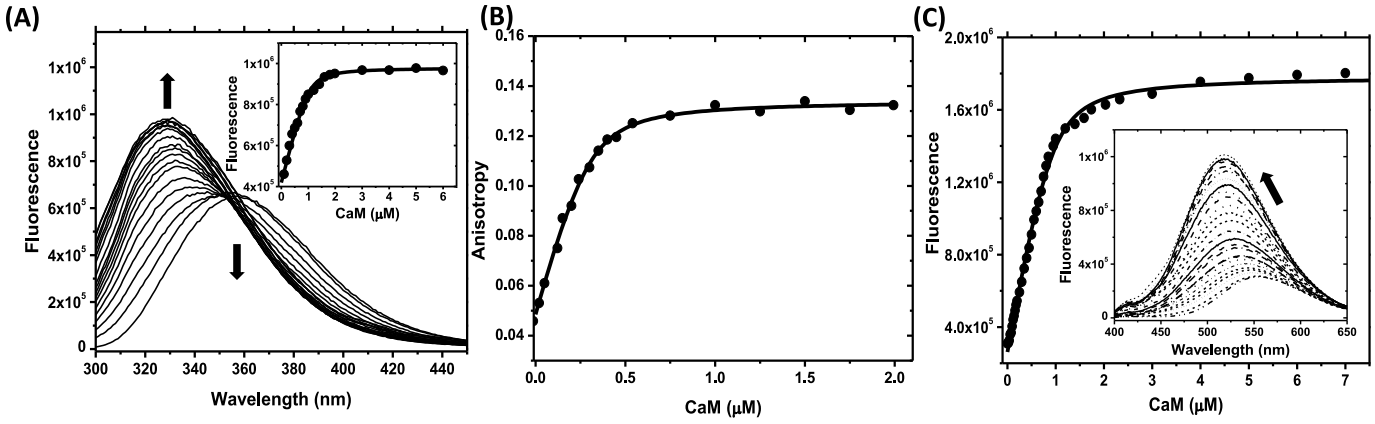

Fig. 1. The CMBD and CaM binding determined by fluorescence in the presence of Ca^{2+}. (A) shows the corrected Trp fluorescence spectra of 2 μM CMBD upon the addition of CaM. The Insert shows the fitting of a plot of the concentration versus the intensity at 330 nm. **(B)** shows the anisotropy measurement of 1 μM CMBD with CaM with the emission at 352 nm. **(C)** shows the Dansyl fluorescence of 2 μM D-CMBD titrated with CaM. The curvature binding curve and slightly more than 1 equivalent of CaM for saturation indicate that the binding is not extremely strong, and CaM is capable of binding more than one ligand.

Table 1
Binding affinities for CaM/CMBD. The binding measurements were conducted in the buffer containing 50 mM Tris, pH 7.5, 2 mM Ca^{2+} at room temperature for fluorescence and at 25°C for ITC.

Binding by Fluorescence (titrant/analyte)	Binding constant (M^{-1})	Stoichiometry ($n_{[Peptide]/[Protein]}$)	
CaM/CMBD (intensity)	$(1.71 \pm 0.60) \times 10^7$	2.10 ± 0.35	
CaM/CMBD (anisotropy)	$(8.64 \pm 2.25) \times 10^6$	1.91 ± 0.24	
CaM/D-CMBD	$(4.95 \pm 1.03) \times 10^6$	2.11 ± 0.11	
Binding by ITC (titrant/analyte)	**Binding constant (M^{-1})**	**Stoichiometry ($n_{[peptide]/Protein]}$)**	**$\Delta H_{protein}$ (kcal/mol)**
CMBD/CaM	(8.78 ± 1.25) x 10^5	1.82 ± 0.08	$- 6.94 \pm 0.04$
CaM/CMBD	(1.02 ± 0.21) x 10^6	1.79 ± 0.11	$- 7.85 \pm 0.06$
CMBD/NCaM	(2.42 ± 1.21) x 10^6	0.89 ± 0.06	$- 3.94 \pm 0.45$
CMBD/CCaM	(9.50 ± 0.62) x 10^5	1.04 ± 0.03	$- 4.02 \pm 0.06$

complexed with CaM, the anisotropy increases up to 0.136. The binding curve is hyperbolic, and the saturation reaches at molar ratio near 1.2, indicating the binding model cannot be 1:1 (Fig. 1B). In fact, the anisotropy fitting yields the K_a and $n_{CMBD/CaM}$ values to be 8.64×10^6 M^{-1} and 1.91. Our data seems to agree with the previous report about binding affinity, but not stoichiometry [18]. However, the large standard deviations from affinity and stoichiometry indicate the difficulty of eliminating the fluorescence from CaM precisely (Table 1).

To avoid the fluorescence from CaM, we used an alternative means to measure the binding. Firstly, we employed an N-terminal Dansyl-labeled CMBD (D-CMBD). Fig. 1C shows the Dansyl fluorescence of the peptide has a maximal emission at 550 nm, which shifts to 518 nm upon CaM binding with ~ 8-fold intensity increases. The fitting yields the K_a and the molar ratio of D-CMBD to CaM (i.e., $n_{D\text{-}CMBD/CaM}$) value to 4.95×10^6 M^{-1} and 2.11 (Table 1). The labeled peptide appears to bind CaM in the absence of Ca^{2+}. The emission spectra are very different to the ones in the presence of Ca^{2+}: the emission maxima and intensity changes are much smaller. The binding affinity was estimated to be ~10^5 M^{-1}, in which the binding is primarily through electrostatic interactions, which are diminished in a higher ionic strength (Fig. S2A&B). A similar finding using CMBD's Trp fluorescence was found in the absence of Ca^{2+} (Fig. S2C). Therefore, we concluded that such a Ca^{2+}-independent interaction is non-specific and not biologically importance because of the high ionic strength (= ~0.25 M) in physiological condition.

3.1.2. Binding determined from isothermal titration calorimetry

We measured the heat evolved from the non-covalent interactions by ITC. When the syringe containing 350 μM CMBD was titrated into a solution containing 25 μM CaM in the presence of 50 mM Tris, 2 mM Ca^{2+}, pH 7.5, at 25°C, an exothermic reaction was observed, and the inflection point of the titration curve revealed that molar ratio ([CBMD]/[CaM]) is near 2 (Fig. 2A). The data was fit well to the model of "one set of sites", yielding the K_a value of 8.78×10^5 M^{-1}, the ΔH value of −3.81 kcal/mol, and the $n_{CMBD/CaM}$ value of 1.82. The results indicate that there are two independent CMBD binding sites for CaM and each has a binding affinity of 8.78×10^5 M^{-1} and heat enthalpy change of −3.81 kcal per mole CMBD (ΔH_{CMBD}). Since we are interested in the molar enthalpy change per CaM (ΔH_{CaM}), it was calculated to be −6.94 kcal/mol (i.e., $\Delta H_{CMBD} \times n_{CMBD/CaM}$). To verify this independent binding, we employed a back-titration by injecting 250 μM CaM into 40 μM CMBD (Fig. 2B); the obtained thermodynamic parameters were consistent to the previous titration, with the K_a value of 1.02×10^6 M^{-1}, ΔH_{CaM} of −7.85 kcal/mol, and $n_{CaM/CMBD}$ of 0.56 (i.e., $n_{CMBD/CaM} = 1.79$). Further, we replaced CaM with its half-domains (NCaM and CCaM) and the binding affinities are comparable with near unity stoichiometry. The enthalpy changes of the half-domains are close to $\Delta H_{CMBD,}$ which was

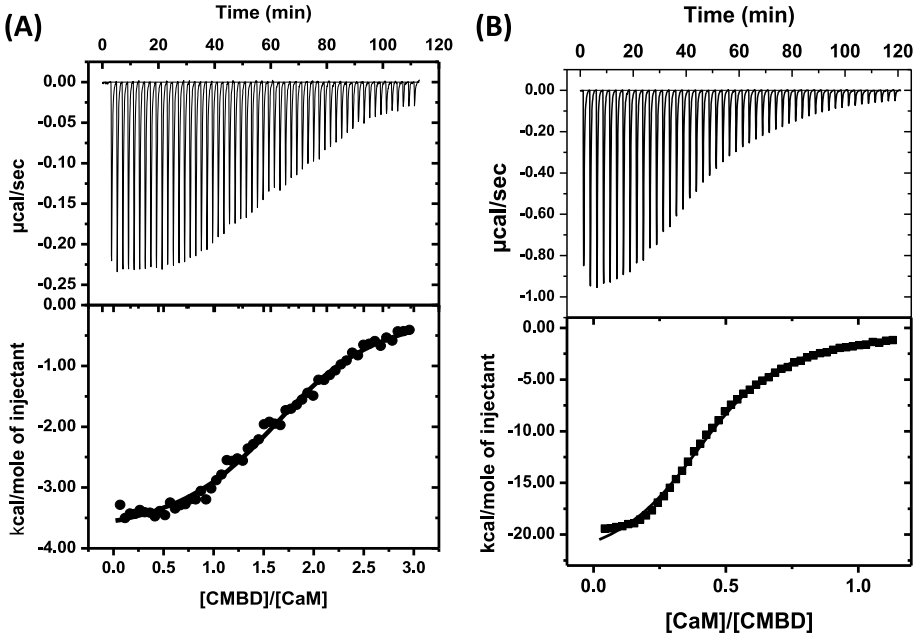

Fig. 2. Binding of CaM and CMBD determined by isothermal titration calorimetry. (A) shows the representation of the titration by adding CMBD to 25 μM CaM in the presence of 50 mM Tris, pH 7.5, 2 mM Ca^{2+} at 25°C. **(B)** shows the representation of the reverse titration by titrating CaM to 40 μM CMBD in an identical condition. The n values from the fitting were 1.834 and 0.521 for (A) and (B), respectively, which are converted to the number of CMBD peptides per CaM tabulated in Table 1.

determined from using intact CaM. In summary, we unambiguously confirmed the binding between CaM and Nox5's CMBD is in the range of 10^6 M^{-1}, and CaM contains two independent CMBD binding sites. The binding is specific and does not change significantly in the presence of 0.1 − 0.25 M NaCl.

3.1.3. The CaM/Nox5's CMBD interaction determined by size-exclusion chromatography

When the binding kinetics of CaM/CMBD complex were measured, we failed to detect any meaningful kinetic traces using a stopped-flow fluorescence device as used previously for the CaM/Orai system [21]. Therefore, our results implied that its association kinetics are much faster than the dissociation rate. We then turned to size exclusion chromatography (SEC) to determine if the complex formation can be observed in a non-equilibrium system. In SEC, high ionic strength in the buffer is essential for a good separation. In the following examples, 0.2 M NaCl was used except as otherwise indicated. The Ca^{2+}-bound CaM (Ca^{2+}-CaM) was eluted as a sharp peak at 9.92 min while apo-CaM was eluted at 9.81 min (Fig. 3A&D), the latter is consistent with a flexible apo-CaM structure. The D-CMBD peptide was used because we can simultaneously monitor its free and CaM-bound forms. D-CMBD was eluted as a broad peak at 29.31 and 25.67 min in the presence of Ca^{2+} and EDTA, respectively (Fig. 3B&D). The CMBD peptide is unstructured as seen in Circular Dichroism (data not shown) and appears to chelate with the Ca^{2+} ions, which forms a more compact peptide. In the presence of Ca^{2+}, Dansyl fluorescence was found be in the fractions corresponding to CaM and the peptide. When a large excess of CaM was included, the CMBD binding is driven to be complete as judged from the Dansyl fluorescence that was only detected from the fractions near ~10 min (Fig. 3C). Because of low separation resolution of the gel filtration, the previously determined stoichiometry cannot be confirmed as D-CMBD is relatively small (~2 kDa). Our results revealed that a stable Ca^{2+}-CaM/CMBD complex was formed in non-equilibrium system. The Dansyl fluorescence was not detected in the CaM fraction in the absence of Ca^{2+} (Fig. 3D).

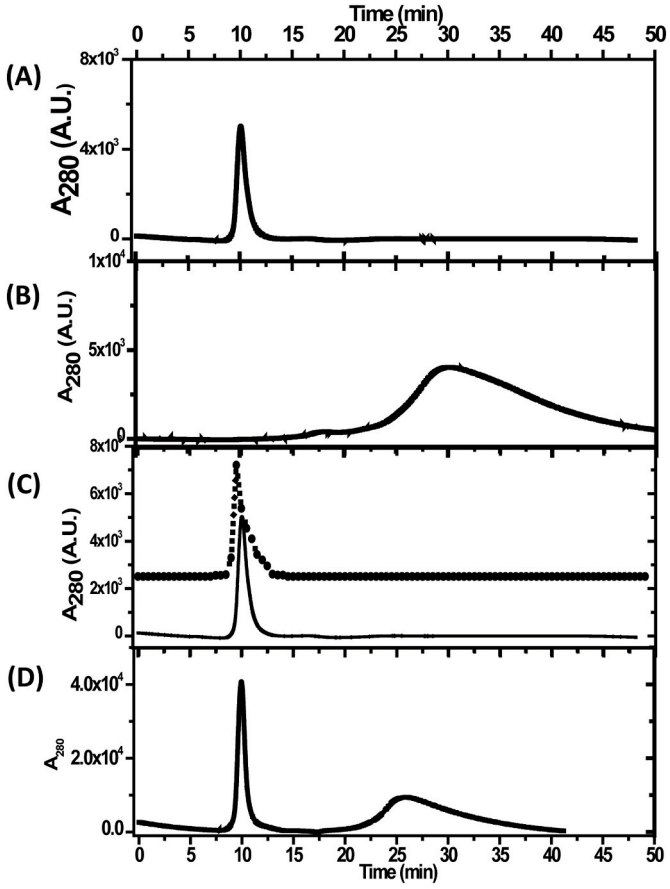

Fig. 3. Size Exclusion Studies of CaM and CMBD peptide binding. The HPLC-SEC was performed in a buffer containing 50 mM Tris, 0.2 M NaCl, 2 mM Ca^{2+} or 1 mM EDTA, pH 7.5. **(A)** and **(B)** show the elution profiles of CaM and D-CMBD, respectively. **(C)** shows that D-CMBD was found to be complexed with Ca^{2+}-CaM when a large excess of CaM was included. The dotted line presents that the fractions exhibited Dansyl fluorescence. **(D)** shows the mixture containing CaM and D-CMBD was separated in the absence of Ca^{2+}. No Dansyl fluorescence was found in the CaM fractions.

3.2. Characterization of the interactions between CaM and Nox5's dehydrogenase domain

3.2.1. Expression of Nox5's partial DH constructs

Since Nox5's DH (residues 403–719) is extremely insoluble and unstable, we attempted to increase its solubility by fusing with thioredoxin, glutathione transferase (GST) or maltose binding protein (MBP). However, they were expressed as an inclusion body, except for the shorter MBP-fused DH constructs. Previously, we have expressed and purified the partial Nox5's DH constructs with MBP attached in their N-terminus, which include the residues 665–719 and 605–719 (*i.e.,* MBP-$DH_{665\text{-}719}$ and MBP-$DH_{605\text{-}719}$). MBP-$DH_{605\text{-}719}$ contains REFBD and CMBD sequences while MBP-$DH_{665\text{-}719}$ contains only the CMBD sequence, which allowed us to conclude that the REFBD sequence is the sole binding site for Nox5's EFD. Here we extended the DH constructs by including the residues 584–719 and 528–719 to generate MBP-$DH_{584\text{-}719}$ and MBP-$DH_{528\text{-}719}$ (Fig. 4), in which we aimed to assess their protein folding in terms of binding to Nox5's EFD and CaM. Further, the longer DH constructs will allow us to extract information such as structural changes. Interestingly, these two constructs were found in higher extent in the soluble portion. All the DH constructs contain the CMBD and REFBD binding sites except MBP-$DH_{665\text{-}719}$ that only contains the CaM binding site. For clarity, we omitted MBP in naming those DH constructs throughout the text.

MBP-fused proteins are typically purified through an amylose column. However, the protein purified by a single chromatography is not sufficient for binding studies, especially for stoichiometry determination. We found that an ion-exchange column (i.e., DEAE-cellulose) prior to and/or CaM-immobilized column after the amylose column significantly increase the purity. An example of the purified $DH_{528\text{-}719}$ is shown in Fig. S3 and only those with sufficient purity were used for biophysical characterization.

Despite of the high purity of the DH proteins as seen in SDS-PAGE, the concentrated samples are only stable for days in the presence of Ca^{2+} at 4°C. The degradation appears to be attributed from the trace amount of the Ca^{2+}-dependent protease(s) that were strongly associated with the MBP-fused DH proteins. Including serine protease inhibitors, such as phenylmethylsulfonyl fluoride (PMSF) or benzamidine, partially suppressed the degradation.

3.2.2. The oligomeric states of DH by SEC and DLS

Since there is evidence that Nox5 formed a oligomer when it was expressed in HEK293 cell line [22], we used SEC to monitor its oligomeric states. When $DH_{584\text{-}719}$ was injected into a gel filtration column equilibrated with 50 mM Tris, pH 7.5, 0.2 M NaCl, we observed a major peak at 6.7 min and a very minor peak near 9.5 min (Fig. 5B). Bovine serum albumin (BSA) running on the same conditions shows three distinct peaks at 8.57, 7.76, and 7.23 min, which are the BSA monomer (66 kDa), dimer (132 kDa), and trimer (198 kDa), respectively. It appears that the first peak containing the heterogenous DH macromolecules with the predominate species having molecular weights larger than BSA trimer. The anticipated MBP-fused $DH_{584\text{-}719}$ monomer is 56 kDa, and it was eluted much later (9.5 min) than the BSA monomer (8.57 min), suggesting that the MBP-fused DH protein has a more compact structure than BSA. In fact, a similar observation was seen in

```
hDH     403MEVNLLPSKVTHLLIKRPPFFHYRPGDYLYLNIPTIARYEWHPFTISSAPEQKDTIWLHI462
csDH    418VNASLLPSKVLGLQVQRPQSFNYQPGDYLFIKCPGISKFEWHPFTISSAPEMPDVLTLHI477

hDH     463RSQGQWTNRLYESFKASDPLGRGSKRLSRSVTMRKSQRSSKGSEILLEKHKFCNIKCYID522
csDH    478RAVGSWTGKLYQLI----------REQREEWIRSGSSQS----------LPGVPVYID515

                 528
hDH     523GPYGTPTRRIFASEHAVLIGAGIGITPFASILQSIMYRHQKRKHTCPSCQHSWIEGVQDN582
csDH    516GPYGTPSTHIFESKYAILICAGIGVTPFASILKSILHRNQQNPAKMP----------562

            584                      605
hDH     583MKLHKVDFIWINRDQRSFEWFVSLLTKLEMDQAEEAQYGRFLELHMYMTSALGKNDMKAI642
csDH    563--LKKVHFYWLNREQKAFEWFVELLSKIEAEDTN-----NLFDLNLYLTGAQQKSDMKSS616

                             665
hDH     643GLQMALDLLANKEKKDSITGLQTRTQPGRPDWSKVFQKVAAE-KKGKVQVFFCGSPALAK701
csDH    617TLFVAMDLMHQETKVDLITGLKSRTKTGRPDWEEIFKDVAKQHAPDNVEVFFCGPTGLAL675

hDH     702VLKGHCEKFGFRFFQENF719
csDH    676QLRHLCTKYGFGYRKENF691
```

Fig. 4. Sequence alignment of human Nox5 DH (hDH) and Cylindrospermum stagnale Nox5 DH (csDH). The arrow keys indicate the start points for the truncated hDH proteins used in this study. The sequence in red is REFBD and the sequence in brown is CMBD. The putative Caveolin binding site of hDH is shown in blue color. (For interpretation of the references to color in this figure legend, the reader is referred to the Web version of this article.)

hemoglobin tetramer (~62 kDa), which was eluted out at 9.51 min in our condition (data not shown). In other words, using BSA as standards for SEC underestimates the molecular weight for compact proteins [23]. The presence of reducing agent DTT and Ca^{2+} ions did not affect its HPLC profile, excluding the possibility of intermolecular disulfide formation and Ca^{2+}-induced oligomer formation.

We then employed Dynamic Light Scattering (DLS) to study the DH, which shows that the decay of the autocorrelation function was substantially longer than 100 μs for $DH_{584\text{-}719}$ (Fig. 5A). The fitting revealed a highly multimeric macromolecule with the hydrodynamic radius (R_h) = 8.3 nm with 42.5% of poly-distribution (%pd). The estimated average molecular weight was ~450 kDa with the assumption of Raleigh sphere for molecules. However, we should point out that the determined molecular weight should be viewed as qualitative because of the limited application using dynamic scattering (instead of static scattering) for molecule wight determination. In comparison, CaM was eluted out at 9.92 min in SEC and has a fast autocorrelation decay. Note that CaM used contains a six-histidine tag and its anticipated molecular weight is 18,132 Da. The fitting gave the R_h value of 2.0 nm (~18 kDa) with the pd% value of 19.5. Since the DH protein is fused with MBP, it is possible that the multimer is due to the self-oligomerization of MBP. However, when the purified MBP was subjected to the SEC and DLS measurements, it was eluted out at 9.55 min and has R_h = 2.6 nm with the %pd of 10.1 at the same settings. Therefore, we concluded that the oligomer formation is attributed to the DH protein, not the MBP.

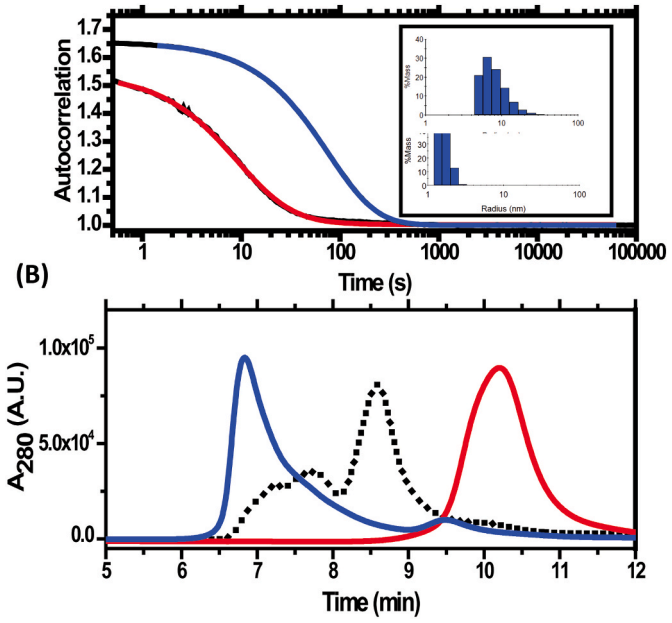

Fig. 5. The oligomeric states of DH and CaM determined by DLS and SEC. **(A)** The autocorrelation functions of 1 mg/mL CaM (Red) and $DH_{584\text{-}719}$ (Blue) in 50 mM Tris, pH 7.5 were measured to determine their sizes and distribution (Insert, Top: $DH_{584\text{-}719}$, bottom: CaM). **(B)** The SEC elution profiles of CaM (18 kDa) and MBP-$DH_{584\text{-}719}$ (56 kDa) were compared with BSA (dotted line) in the presence of 50 mM Tris, pH 7.5, 0.2 M NaCl. (For interpretation of the references to color in this figure legend, the reader is referred to the Web version of this article.)

To further study the possible oligomeric states, we included mild chaotropic agent (2 M urea) to dissociate the $DH_{584\text{-}719}$ oligomer partially. We observed four distinct peaks at 6.71, 7.25, 8.02, and 9.52 min (Fig. 6A). We assigned the Species 1 and 2 at 9.52 and 8.02 min to be DH monomer and dimer, respectively, while the Species 3 at 7.25 min was assigned to be DH trimer (~168 kDa) and the Species 4 at 6.71 min to be tetramer (~224 kDa). Note that these assignments are for the presentation purpose as the resolution from our SEC and DLS cannot determine the oligomeric states precisely. We found that all other DH constructs have dominant trimer and tetramer species (or Species 3 and 4) with small amounts of monomer and dimer species. The equilibrium between these two dominant species depends on the ionic strength. For example, the tetramer species is dominated in a buffer with a lower ionic strength (e.g., in the presence of 0.2 M NaCl); but the trimer species is a major form in the high ionic strength buffer containing >0.25 M NaCl (Fig. 6B). A significant tetramer formation was also found when DH concentrations were higher. (Fig. 6B).

Next, we studied the interaction of CaM and DH using HPLC-SEC. Since the $DH_{584\text{-}719}$ and $DH_{528\text{-}719}$ are significantly larger than the other shorter constructs, they are separated from CaM better in SEC. We only showed their results here despite of a similar trend for all constructs. When 50 μM $DH_{584\text{-}719}$ and 10–50 μM CaM were mixed in presence of Ca^{2+}, the elution profile revealed a new peak with the

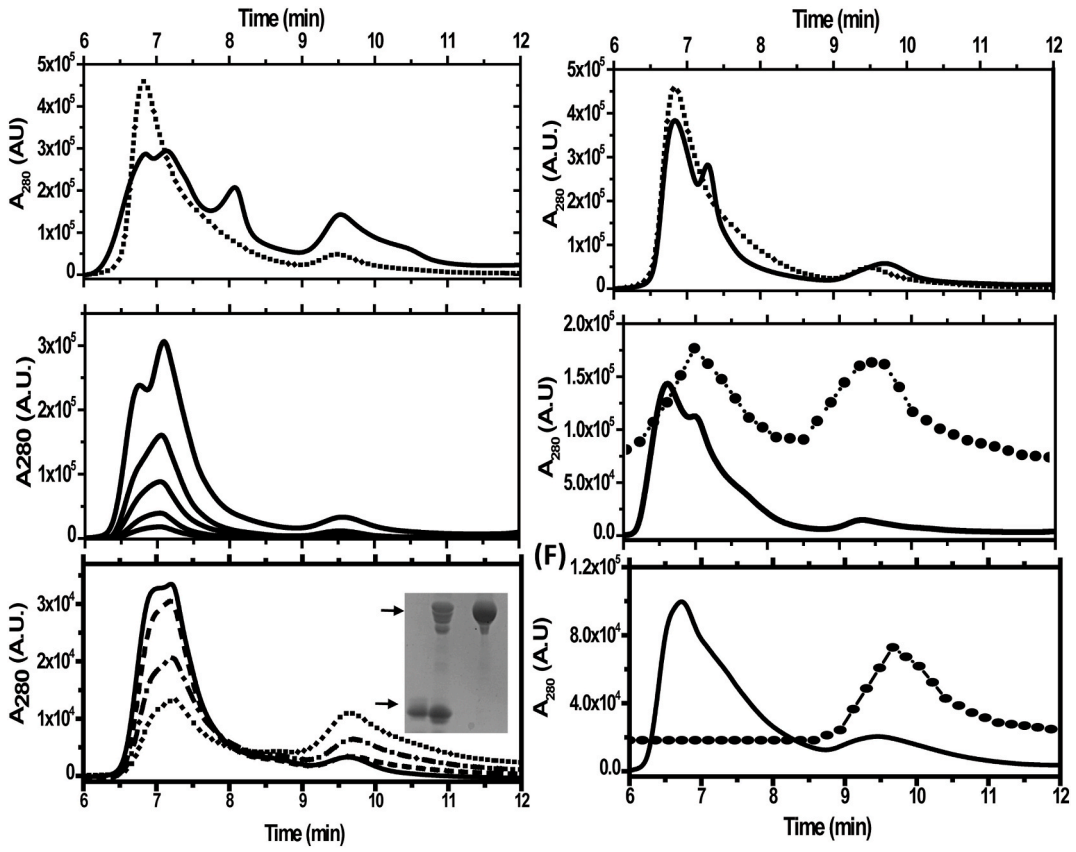

Fig. 6. Size Exclusion chromatography for the interaction of CaM and DH. **(A)** shows the $DH_{584-719}$ in the absence (dotted line) and presence (solid line) of 2 M urea in 50 mM Tris, pH 7.5, 0.2 M NaCl. The notations for M, D, Tri, and Tetra are for monomer, dimer, trimer, and tetramer, respectively. **(B)** shows the effects of ionic strength and concentration on the DH oligomeric states. A 20 μL of the different concentrations of $DH_{584-719}$ (43, 87, 175, 350, ad 700 μM) was subjected to SEC in a higher ionic strength (>0.25 M NaCl), in which the condition favors trimer formation. **(C)** shows the 20 μL of the samples incubated overnight at 4°C containing 45 μM $DH_{584-719}$ and 45 (solid), 90 (dashed line), 120 (dash-dotted line), or 180 μM CaM (dotted line) were injected into a HPLC-SEC in a buffer containing 0.2 M NaCl and 2 mM Ca^{2+}. The insert shows the SDS-PAGE from the samples containing CaM (Lane 1), $DH_{584-719}$ (Lane 3) and the mixture of $DH_{584-719}$ and CaM (1:2 ratio) after 30 min incubation at RT (Lane 2). **(D)** shows the samples containing 50 μM $DH_{584-719}$ alone (dotted line) and plus 50 μM CaM (solid line) in a buffer containing 50 mM Tris, pH 7.5, 0.2 M NaCl, 2 mM Ca^{2+}. **(E)** shows that same reaction condition as in (D) except that $DH_{528-715}$ and D-CaM were used. Note that the multimers of the larger $DH_{528-719}$ (MW = ~62 kDa) were eluted earlier than $DH_{584-719}$. The elution fractions were subjected to Dansyl fluorescence measurement (dotted line with symbols). **(F)** shows an identical reaction condition as in (E) except that the buffer contains 1 mM EDTA.

elution time at 7.2 min, corresponding to a molecular weight comparable to that of trimer (Fig. 6D). Furthermore, the dimer disappeared as judged by the disappearance of the shoulder near 8 min. To confirm the change is due to CaM binding, we replaced CaM with D-CaM and performed a similar measurement. When the equal amounts of D-CaM and $DH_{528-719}$ were mixed and injected to HPLC (Fig. 6E), the eluted fractions were subjected to the Dansyl fluorescence measurements, where approximately half of the D-CaM was found in the fractions containing DH while the other half remains in the unbound form. The DH-bound D-CaM was also evidenced by its maximal emission wavelength at 500 nm while D-CaM alone showed the λ_{max} value at 516 nm (Fig. 8A). While we cannot obtain stoichiometry information in SEC, we anticipated that including a large excess of CaM should shift the equilibrium solely toward the CaM/DH complex, if it is stable in a non-equilibrium system. It was surprising to us that when including higher amount of CaM (e.g., >2 folds) or long incubation time (Fig. S4) resulted in a significant decrease in the multimer and increase in the fractions corresponding to the DH monomer (Fig. 6C), the latter was determined to be the products of degradation (Insert in Fig. 6C). Though it is unclear the source and types of contaminated proteases, Ca^{2+}-CaM speeds up the degradation by opening the DH structure to become accessible for proteases, in which the rate of degradation depends on the amount of CaM present in solution (i.e., the ratio of DH and CaM). As expected, we did not observe any Dansyl fluorescence in the DH fractions in the absence of Ca^{2+} (Fig. 6F).

3.2.3. *Pulldown experiments revealed that both half-domains of CaM interact with DH constructs*

In the peptide-model study, CaM binding to CMBD peptide involves its two half-domains. To determine whether this is the case for DH, pulldown experiments were conducted. Fig. 7 shows that when $DH_{665-719}$ was loaded into a column immobilized with CFP-CaM followed by elution with EDTA solution (for chelating Ca^{2+} ions). As expected, the binding of CaM and $DH_{665-719}$ was only observed in the presence of Ca^{2+}. When the immobilized CaM was replaced with N- and C-terminal half domains of CaM (NCaM and CCaM), $DH_{665-719}$ was retained in the column in the presence of Ca^{2+}, supporting that both half lobes of CaM participate in the binding to DH. The similar reproducible results were observed for all DH constructs.

3.2.4. *Studies of CaM binding to DH constructs by fluorescence and ITC*

To study the CaM-DH interaction by fluorescence, we prepared Dansyl-labeled CaM (D-CaM) [21] and determined its binding to all Nox5's DH constructs by fluorescence spectroscopy. Fig. 8A is a representation of a solution of $DH_{665-719}$ that was titrated into a solution containing 2 μM D-CaM in the presence of Ca^{2+}. The fluorescence increases and the maximal emission wavelength (λ_{max}) is shifted from 510 to 480 nm, a significant difference to the D-CaM/CMBD system that

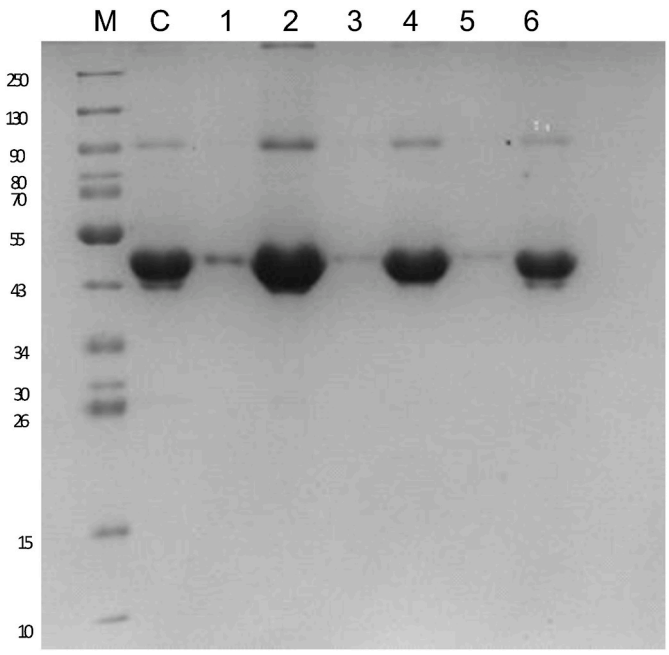

Fig. 7. Pulldown experiment showing the interaction between Ca^{2+}-CaM and $DH_{665-719}$. A solution containing 1.0 mg MBP-fused $DH_{665-719}$ (Lane C; M.W. = ~49.2 kDa) was loaded into columns immobilized with fluorescent protein fused CaM, NCaM, and CCaM in the presence of Ca^{2+} (Lane 2, 4, 6) and EDTA (Lane 1, 3, 5). After washing, the proteins were eluted with EDTA and run on a 12% SDS-PAGE.

shows a very small intensity (Fig. S5). The result suggests that the microenvironment of Dansyl group in CaM is more protected when bound with DH than with CMBD. We fit the titration data and obtained the K_a value of 4.90 × 10^6 M^{-1} with near unity stoichiometry (Fig. 8A lower panel). Including up to 0.25 M NaCl resulted in only a small decrease in binding affinity. Contrast to the CaM/CMBD system, we did not observe any Dansyl fluorescence intensity changes in the absence of Ca^{2+}. The binding measurements for other DH constructs are tabulated in Table 2.

Additionally, we employed ITC to determine binding constants and enthalpy changes. When a solution of CaM was titrated into 20–50 μM $DH_{605-719}$, the binding is exothermic and the affinity was determined to be in the range of 10^6 M^{-1}, but the stoichiometry ($n_{CaM/DH}$) is significantly lower than 1 (Fig. S6A). The low stoichiometry was not expected. Interestingly, there is a correlation between the obtained n values and the concentrations of DHs used (Fig. S6B). In fact, the low stoichiometry was due to the DH degradation during the process for sample preparation and the ITC measurements (the total time was more than 4 h), evidenced by a notable baseline drift in the uncorrected baseline in ITC (Insert in Fig. S6A). It is possible that the higher amounts of DH used contained more contaminated proteases, which renders DH more degradable when CaM was titrated.

When the DH concentrations were near 2 μM range, the binding affinity was determined to be ~5 x10^6 M^{-1} with a stoichiometry near one and the ΔH_{CaM} of −8.2 kcal/mol (Fig. 8B&C and Table 2). The obtained unity stoichiometry is consistent with that obtained from fluorescence, indicating that the DH degradation was insignificant in this condition (otherwise, we should see the stoichiometry is less than 1 because of less DH available for CaM binding). Our results also revealed that $DH_{665-719}$ has a lower heat enthalpy value, which is comparable to the peptide-based study, while the larger constructs have more negative enthalpy changes, indicating a conformational change that renders more non-covalent interactions (Table 2).

4. Discussion and conclusion

To better understand the binding mechanism for CaM and Nox5, we revisited the system by studying the interactions between CaM and the

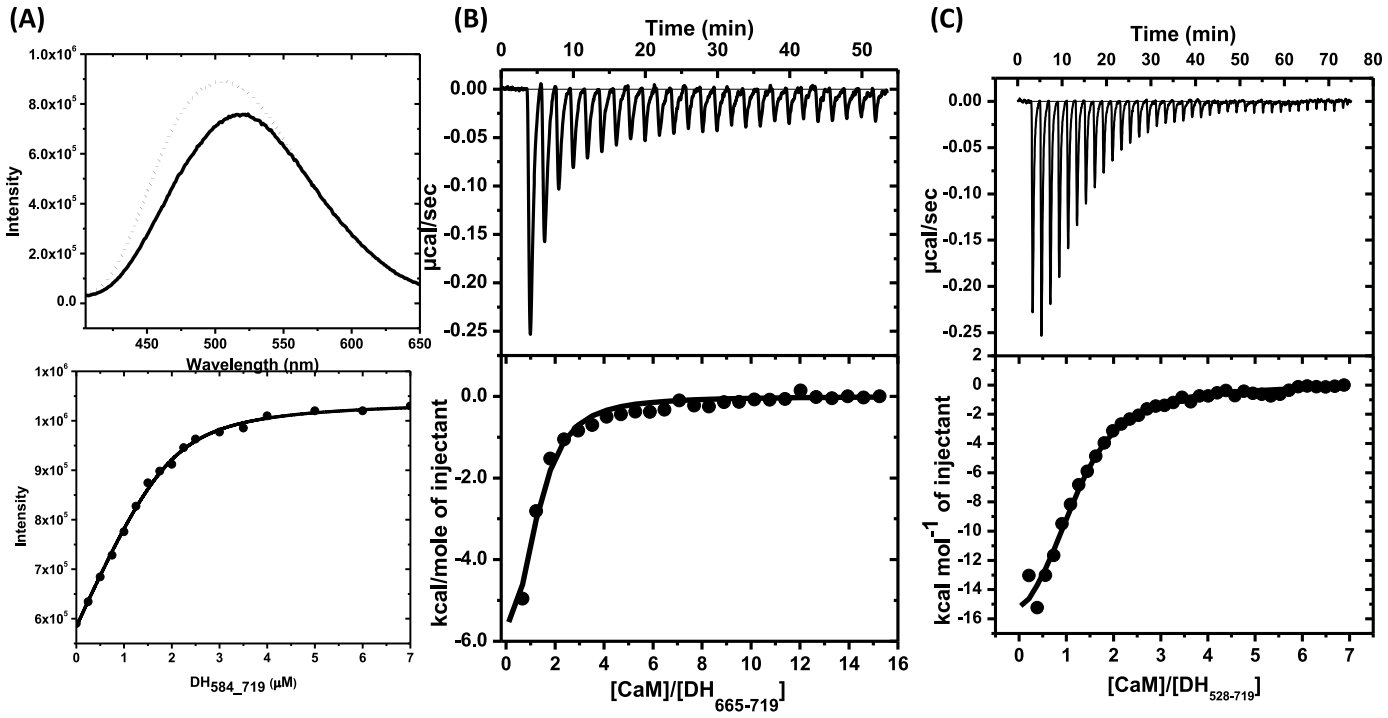

Fig. 8. CaM Binding to DH determined by fluorescence and ITC. (A) shows a representation of a solution of $DH_{665-719}$ that was titrated into a solution containing 2 μM D-CaM in the presence of Ca^{2+}. The initial and final scans show the blue shift in emission wavelength (Upper Panel). The lower panel shows the resulting fitting. **(B)** shows the representation of the binding for the titration of 0.2 mM CaM to 2.5 μM $DH_{665-719}$ in the presence of 50 mM Tris, pH 7.5, 2 mM Ca^{2+} at 25°C. **(C)** shows the titration by adding 0.1 mM CaM to 2 μM $DH_{528-719}$ in an identical condition. The average values of K_a and n are tabulated in Table 2.

Table 2
The CaM binding to DHs by fluorescence and ITC in the presence of 50 mM Tris, pH 7.5, 2 mM Ca^{2+}.

Binding by Fluorescence (titrant/analyte)	Binding constant (M^{-1})	Stoichiometry ($n_{[Peptide]/[Protein]}$)	
$DH_{665-719}$/D-CaM	$(4.90 \pm 0.28) \times 10^6$	0.92 ± 0.10	
$DH_{605-719}$/D-CaM	$(2.52 \pm 0.51) \times 10^6$	1.02 ± 0.23	
$DH_{584-719}$/D-CaM	$(1.82 \pm 0.43) \times 10^6$	0.89 ± 0.32	
$DH_{528-719}$/D-CaM	$(1.39 \pm 0.21) \times 10^6$	0.92 ± 0.24	
Binding by ITC (titrant/analyte)	**Binding constant (M^{-1})**	**Stoichiometry ($n_{[peptide]/Protein]}$)**	**ΔH_{DH} (kcal/mol)**
CaM/$DH_{665-719}$	$(1.39 \pm 0.26) \times 10^6$	1.15 ± 0.07	-8.21 ± 1.62
CaM/$DH_{605-719}$	$(8.94 \pm 0.65) \times 10^5$	1.15 ± 0.02	-14.80 ± 1.71
CaM/$DH_{584-719}$	$(9.33 \pm 0.15) \times 10^5$	1.04 ± 0.16	-16.75 ± 2.23
CaM/$DH_{528-719}$	$(2.71 \pm 0.23) \times 10^6$	1.18 ± 0.05	-18.96 ± 1.25

Nox5's CMBD peptide using intrinsic/extrinsic fluorescence and isothermal titration calorimetry. The fluorescence characterization indicates that the Trp residue of CMBD becomes buried in a non-polar environment and, therefore, protected from dynamic quenching upon Ca^{2+}-CaM binding. Without Ca^{2+}, CaM binds the CMBD peptide via non-specific electrostatic interaction which is not biologically significant. The binding affinity for the CaM/CMBD was determined to be more precisely in the range of 10^6 M^{-1} by extrinsic fluorescence and ITC, about half to one-order lower than the previous reported value. However, CaM binds two CMBD peptides using its half-domains with similar interactions (e.g., similar binding enthalpy); no cooperativity was observed. Previously, we hypothesized that the extent of the hydrophobic changes from the ANS fluorescence provides information on the mode of CaM binding to its targeted peptides [11]. The "collapsed" form of Ca^{2+}- and CMBD-bound CaM would have a substantial ANS fluorescence decrease while the "extended" form has less significant change. ANS fluorescence of CaM/CMBD decreases ~3% and therefore, we hypothesized that Ca^{2+}-CaM binds two Nox5's CMBD peptides in an extended structure [11], further supported by a small intensity change for D-CaM/CMBD (Fig. S5).

The conclusion from our solution study here is consistent with a recently published crystal structure [17], in which the peptide-bound CaM has an identical structure to Ca^{2+}-CaM (the "extended" structure), and each of the two CMBD peptides is bound in the cleft formed in half-domain. Interestingly, the crystal structure show that the CaM's N-terminal lobe binds to the C-terminal half of one CMBD peptide while its C-terminal lobe binds to the N-terminal half of the other CMBD peptide. Though one can argue that the determined stoichiometry from the fitting largely depends on the accuracy of the concentrations used for fitting, here we have used different characterizations but yielded consistent results. A more concrete approach to confirm this is to generate, for instance, an MBP-fused CMBD protein (MBP-CMBD) and to determine whether a larger complex containing one CaM and two MBP-CMBD can be seen in SEC. Unfortunately, such a protein construct was not expressed in our system.

Next, we studied the interaction using the truncated DH constructs. Though Nox5's DH is not soluble in bacterial expression system, four soluble MBP-fused DH truncated forms were obtained in a large quantity with $DH_{528-719}$ found most soluble, which may be due to that it forms a stable subdomain as shown in the modeled structure based on the DH of *Cylindrospermum stagnale* Nox5 (csNox5's DH) (Fig. 9A). All DH constructs appear to be folded correctly. Their CMBD sequence is accessible to CaM, and the binding affinity is comparable to the study from the CaM/CMBD system except the stoichiometry, in which we found a ratio of 1:1 for CaM:DH. The study using DH for CaM binding is not trivial since the csDH has the CMBD region (Fig. 4) formed as a helical structure. Because of the conformation, several key residues of CMBD interacting with CaM are buried and, therefore, no CaM binding was observed which is reasonable to conclude that CaM does not play a role for *cs*Nox5 because of lacking CaM in bacteria. Because csDH has been found as monomer in crystallography [24], we hypothesized that the CMBD sequence partially buried in hDH monomer becomes exposed upon oligomerization. The unity stoichiometry determined by using micromolar DH suggests that the binding mode of CaM to Nox5 is different to the peptide-based system. It is likely that CaM binds to the CMBD region of DH in a "collapsed" model as seen in the complex formed by CaM and CMBD of eNOS [11]. An indication is from the significant Dansyl fluorescent change for D-CaM/DH compared with

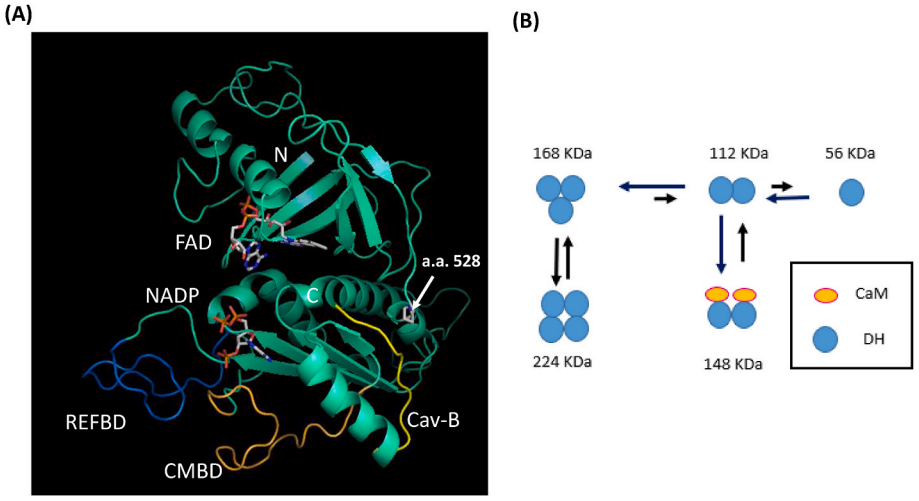

Fig. 9. The human NOX5's DH modeled structure and the oligomeric States of Nox5's DH. **(A)** shows the Nox5's DH structure modeled as previously except the CMBD sequence (Orange) was shown as a random coil. Adjacent to CMBD are REFBD site (Blue) for Nox5's EFD binding and Cav-B site (Yellow) for caveolin binding. Note that the structure of Cav-B appears to be artifactual since there are eight additional residues PWLELAAA (not shown in the model) were added immediately after the C-terminal end of csDH for FAD binding [24]. In hDH, these three elements are structurally close and binding to one likely affects the binding to the others. The arrow indicates the 1st residue in $DH_{528-719}$ that was found most soluble. **(B)** shows the equilibrium between oligomeric states for hDH. The assignments are based on the MBP-fused $DH_{584-719}$ (56 kDa). The predominated species for the expressed DH are trimer and tetramer, in which the equilibrium is affected by concentration and ionic strength. The 1:1 stoichiometry for CaM (18 kDa) binding to DH was determined by ITC and fluorescence, and the binding stabilized the dimeric DH as seen in SEC. (For interpretation of the references to color in this figure legend, the reader is referred to the Web version of this article.)

that of D-CaM/CMBD.

Our data is also consistent with the previous report, in which Nox5 expressed in HEK293 cells is an oligomer, possibly tetramer. The authors suggest that Nox5 form an oligomer through its DH domain, and such multimerization is required for the Nox5's s activity [22]. Based on our data, we proposed the role of CaM in the DH oligomeric states as shown in Fig. 9B. The Nox5's DH are expressed as oligomers, which is Ca^{2+}-independent. Human Nox5's DH is possibly in the forms of trimer and tetramer, in which its equilibrium is concentration and ionic strength dependent. CaM binding appears to stabilize the DH dimeric form. How the oligomeric states of Nox5 related to its superoxide generating activity are largely unclear. Since the shortest truncated DH protein, $DH_{665\text{-}719}$, was also expressed as oligomers, it suggests that the region after the CMBD sequence is crucial for oligomer formation.

It is interesting that the C-terminal end of hNox5 contains a binding site for caveolin-1 (Cav-1) (Figs. 4 & 9A), which is responsible for its localization in the caveola structure. The Cav-1 binding sequence (Cav-B) shares a conserved sequence- ΦXΦXXXXΦ or ΦXXXXΦXXΦ (Φ is an aromatic amino acid and X is any residue). The peptide from the scaffold domain of Cav-1 (Cav-1P) has been shown to inhibit the Nox5's superoxide-generating activity [13]. Because the C-terminal end of csNox5 does not contain Cav-B sequence (Fig. 4) and is found to be a monomer in crystal structure, we suspect that this nonpolar c-terminal end may also play a role in oligomer formation. A closely related hemoflavoprotein protein, nitric oxide synthase (Nos), contains the CMBD (residues 492–511 in endothelial NOS (eNOS)) and Cav-B (residues 350–358 in bovine eNOS) sequences [25]. It has been shown that a Cav-1p (residues 82–101) inhibits the NO production [26]. The NO activity is completely restored by CaM binding [27,28]. Therefore, the role of CaM in Nox5, in addition to increasing Ca^{2+}-sensitivity, may be crucial for lifting inhibitory effect by Cav-1. How the interplay among Nox5, CaM, and Cav-1 in related to Nox5's oligomeric state is largely unknown.

Fig. 9A shows the modeled hDH based on the structure of csDH using homolog modeling [11], except its CMBD sequence was modeled as a random coil to allow the interaction with CaM. In this model, the sequences of REFBD (recognized by Nox5's EFD), CMBD (bound by CaM) and Cav-B (for Cav-1 binding) are close each other in the primary sequence and three-dimensional structure, suggesting the binding to one of each element possibly affects the others. Interestingly, our result seems to support this hypothesis, at least for the conformational changes between REFBD and CMBD. For example, the heat enthalpy changes for CMBD-and-REFBD containing DH constructs (i.e., $DH_{605\text{-}719}$, $DH_{584\text{-}719}$, and $DH_{528\text{-}719}$) is approximately double than that of CMBD-containing $DH_{665\text{-}719}$, indicating an induced conformational change occurred. Furthermore, a conformational change included by Ca^{2+}-CaM binding has rendered the DH proteins more accessible for protease degradation. The interplay among those components with their associated proteins appears to be crucial to activate and regulate the Nox5 superoxide-generating activity. How these bindings are relevant to oligomeric states are equally unclear. However, our result provides insights for Nox5's DH oligomeric states and its related structural changes that are crucial to understand the No5's activation and regulation mechanism.

Funding

This work is partly supported by the grant from the National Science Foundation grant CHE-1608484 to C.-C.W.

Declaration of competing interest

The authors declare that they have no competing interests.

Acknowledgements

We thank the internal financial supports from Southern Illinois University Edwardsville: Research Grants for Graduate Students (RGGS) to DS, LL, and PR and Competitive Graduate Award (CGA) to DS.

Appendix A. Supplementary data

Supplementary data to this article can be found online at https://doi.org/10.1016/j.bbrep.2021.101198.

References

[1] S. Sorce, K.H. Krause, NOX enzymes in the central nervous system: from signaling to disease, Antioxidants Redox Signal. 11 (10) (2009) 2481–2504.
[2] A.S. Kamiguti, L. Serrander, K. Lin, R.J. Harris, J.C. Cawley, D.J. Allsup, J. R. Slupsky, K.H. Krause, M. Zuzel, Expression and activity of NOX5 in the circulating malignant B cells of hairy cell leukemia, J. Immunol. 175 (12) (2005) 8424–8430.
[3] S.S. Brar, Z. Corbin, T.P. Kennedy, R. Hemendinger, L. Thornton, B. Bommarius, R. S. Arnold, A.R. Whorton, A.B. Sturrock, T.P. Hueckstead, et al., NOX5 NAD(P)H oxidase regulates growth and apoptosis in DU 145 prostate cancer cells, Am. J. Physiol. Cell Physiol. 285 (2) (2003) C353–C369.
[4] M. Holl, R. Koziel, G. Schafer, H. Pircher, A. Pauck, M. Hermann, H. Klocker, P. Jansen-Durr, N. Sampson, ROS signaling by NADPH oxidase 5 modulates the proliferation and survival of prostate carcinoma cells, Mol. Carcinog. (2015).
[5] T.J. Guzik, W. Chen, M.C. Gongora, B. Guzik, H.E. Lob, D. Mangalat, N. Hoch, S. Dikalov, P. Rudzinski, B. Kapelak, et al., Calcium-dependent NOX5 nicotinamide adenine dinucleotide phosphate oxidase contributes to vascular oxidative stress in human coronary artery disease, J. Am. Coll. Cardiol. 52 (22) (2008) 1803–1809.
[6] C. Jha Jay, M.D. Watson Anna, G. Mathew, C. de Vos Lisanne, K. Jandeleit-Dahm, The emerging role of NADPH oxidase NOX5 in vascular disease, Clin. Sci. 131 (10) (2017) 981–990.
[7] R.M. Touyz, A. Anagnostopoulou, L.L. Camargo, F.J. Rios, A.C. Montezano, Vascular biology of superoxide-generating NADPH oxidase 5-implications in hypertension and cardiovascular disease, Antioxidants Redox Signal. 30 (7) (2019) 1027–1040.
[8] J.D. Lambeth, Nox/Duox family of nicotinamide adenine dinucleotide (phosphate) oxidases, Curr. Opin. Hematol. 9 (1) (2002) 11–17.
[9] J.D. Lambeth, T. Kawahara, B. Diebold, Regulation of Nox and Duox enzymatic activity and expression, Free Radic. Biol. Med. 43 (3) (2007) 319–331.
[10] J.C. Jha, C. Banal, J. Okabe, S.P. Gray, T. Hettige, B.S.M. Chow, V. Thallas-Bonke, L. De Vos, C.E. Holterman, M.T. Coughlan, et al., NADPH oxidase Nox5 accelerates renal injury in diabetic nephropathy, Diabetes 66 (10) (2017) 2691–2703.
[11] C.C. Wei, E. Hay, D. Smith, L. Lloyd, G. Acharya, R. Ngo, Binding of Nox5's EF-Hand domain to the peptides corresponding to the phosphorylatable region and regulatory inhibitory loop in its dehydrogenase domain, Biophys. Chem. 262 (2020) 106379.
[12] B. Banfi, F. Tirone, I. Durussel, J. Knisz, P. Moskwa, G.Z. Molnar, K.H. Krause, J. A. Cox, Mechanism of Ca2+ activation of the NADPH oxidase 5 (NOX5), J. Biol. Chem. 279 (18) (2004) 18583–18591.
[13] F. Chen, S. Barman, Y. Yu, S. Haigh, Y. Wang, S.M. Black, R. Rafikov, H. Dou, Z. Bagi, W. Han, et al., Caveolin-1 is a negative regulator of NADPH oxidase-derived reactive oxygen species, Free Radic. Biol. Med. 73 (2014) 201–213.
[14] F. Chen, S. Haigh, Y. Yu, T. Benson, Y. Wang, X. Li, H. Dou, Z. Bagi, A.D. Verin, D. W. Stepp, et al., Nox5 stability and superoxide production is regulated by C-terminal binding of Hsp90 and CO-chaperones, Free Radic. Biol. Med. 89 (2015) 793–805.
[15] A. El Jamali, A.J. Valente, J.D. Lechleiter, M.J. Gamez, D.W. Pearson, W. M. Nauseef, R.A. Clark, Novel redox-dependent regulation of NOX5 by the tyrosine kinase c-Abl, Free Radic. Biol. Med. 44 (5) (2008) 868–881.
[16] J.M. Shifman, M.H. Choi, S. Mihalas, S.L. Mayo, M.B. Kennedy, Ca2+/calmodulin-dependent protein kinase II (CaMKII) is activated by calmodulin with two bound calciums, Proc. Natl. Acad. Sci. U. S. A. 103 (38) (2006) 13968–13973.
[17] E. Millana Fananas, S. Todesca, A. Sicorello, L. Masino, P. Pompach, F. Magnani, A. Pastore, A. Mattevi, On the mechanism of calcium-dependent activation of NADPH oxidase 5 (NOX5), FEBS J. 287 (12) (2020) 2486–2503.
[18] F. Tirone, J.A. Cox, NADPH oxidase 5 (NOX5) interacts with and is regulated by calmodulin, FEBS Lett. 581 (6) (2007) 1202–1208.
[19] A.P. Yamniuk, H. Ishida, D. Lippert, H.J. Vogel, Thermodynamic effects of noncoded and coded methionine substitutions in calmodulin, Biophys. J. 96 (4) (2009) 1495–1507.
[20] C.C. Wei, N. Reynolds, C. Palka, K. Wetherell, T. Boyle, Y.P. Yang, Z.Q. Wang, D. J. Stuehr, Characterization of the 1st and 2nd EF-hands of NADPH oxidase 5 by fluorescence, isothermal titration calorimetry, and circular dichroism, Chem. Cent. J. 6 (1) (2012) 29.
[21] D. Jensen, N. Reynolds, Y.P. Yang, S. Shakya, Z.Q. Wang, D.J. Stuehr, C.C. Wei, The exchanged EF-hands in calmodulin and troponin C chimeras impair the Ca(2)(+)-induced hydrophobicity and alter the interaction with Orai1: a spectroscopic, thermodynamic and kinetic study, BMC Biochem. 16 (2015) 6.

[22] T. Kawahara, H.M. Jackson, S.M. Smith, P.D. Simpson, J.D. Lambeth, Nox5 forms a functional oligomer mediated by self-association of its dehydrogenase domain, Biochemistry 50 (12) (2011) 2013–2025.
[23] March 04 Wyatt Technology, Characterization of Hemoglobin Using SEC-MALS Technology, News-Medical, 2021. Retrieved on November 02, 2021 from, https://www.news-medical.net/whitepaper/20140801/Characterization-of-Hemoglobin-using-SEC-MALS-Technology.aspx.
[24] F. Magnani, S. Nenci, E. Millana Fananas, M. Ceccon, E. Romero, M.W. Fraaije, A. Mattevi, Crystal structures and atomic model of NADPH oxidase, Proc. Natl. Acad. Sci. Unit. States Am. 114 (26) (2017) 6764–6769.
[25] G. García-Cardeña, P. Martasek, B.S. Masters, P.M. Skidd, J. Couet, S. Li, M. P. Lisanti, W.C. Sessa, Dissecting the interaction between nitric oxide synthase (NOS) and caveolin. Functional significance of the nos caveolin binding domain in vivo, J. Biol. Chem. 272 (41) (1997) 25437–25440.
[26] S. Ghosh, R. Gachhui, C. Crooks, C. Wu, M.P. Lisanti, D.J. Stuehr, Interaction between caveolin-1 and the reductase domain of endothelial nitric-oxide synthase. Consequences for catalysis, J. Biol. Chem. 273 (35) (1998) 22267–22271.
[27] J.B. Michel, O. Feron, D. Sacks, T. Michel, Reciprocal regulation of endothelial nitric-oxide synthase by Ca2+-calmodulin and caveolin, J. Biol. Chem. 272 (25) (1997) 15583–15586.
[28] J.B. Michel, O. Feron, K. Sase, P. Prabhakar, T. Michel, Caveolin versus calmodulin. Counterbalancing allosteric modulators of endothelial nitric oxide synthase, J. Biol. Chem. 272 (41) (1997) 25907–25912.